Inverse Dynamics of a Hexa Parallel Robot Based on the Principle of Virtual Work

Diego. Nunez[1,3]*, Mauricio. Mauledoux[1], Oscar. Aviles[1], and Adriana. Nino[2]

[1] Grupo de Investigación DAVINCI, Facultad de Ingeniería , Universidad Militar Nueva Granada, Bogota, Colombia
[2] Escuela de Ingeniería Química, Universidad del Valle, Cali, Colombia
[3] Escuela de Ingeniería Mecánica, Universidad del Valle, Cali, Colombia
Email: danvmoldes@gmail.com (D.N); mauricio.mauledoux@unimilitar.edu.co (M.M);
oscar.aviles@unimilitar.edu.co (O.A.); adriana.nino@correounivalle.edu.co (A.N.)
*Corresponding author

***Abstract*—This paper presents a process for solving the inverse dynamics of a parallel kinematic mechanism named Hexa, which consists of six arms with rotational, universal, and spherical joint configurations with six degrees of freedom. The methodology is based on D'Alembert's principle combined with the virtual work principle and the concept of link Jacobian matrices. The virtual works generated by the external and inertial forces were analyzed separately and then combined to facilitate the calculation. The novelty of this work is twofold. First, the derivation of Hexa dynamical equations of motion can be reduced to a system of six equations. Second, these equations can be validated using a virtual physical model. These equations are the basis of the control strategy and support the mechanism optimization design.**

***Keywords*—parallel robot, dynamics model, virtual work, D'Alembert's principle, six degree of freedom**

I. Introduction

Parallel Robots (PR) consist of a moving platform linked to a fixed base through different links that comprise a structure known as a closed kinematic chain. These robots have some advantages over serial manipulators, such as a better weight-to-torque ratio and greater accuracy in applications that require high velocity and acceleration. Some of the applications include flight simulators, manufacturing lines, and rehabilitation devices [1].

Some configurations of parallel robots include the Delta robot [2], Stewart platform [3], Hexa, among others [4]. The Hexa configuration has six Degrees of Freedom (DoFs) and consists of a moving platform and a fixed platform connected through six arms with spherical, universal, and rotational joints. One of the advantages of this configuration is that each arm is supported by a single motor, which reduces system inertia. Similarly, in a comparison to other parallel mechanisms, its workload is one of its greatest assets [5].

The dynamic analysis considers the parameters of structural elements of the mechanisms, such as the mass and moment of inertia, to determine their behavior. There are two approaches to dynamic analysis: direct and inverse. Direct analysis determines the movement parameters against specific forces. Conversely, inverse analysis determines the necessary forces to ensure the desired movement.

The solution to this problem is important for the design and control point as well as its simulation and real-time application. In many cases, the design of parallel robots must to be concurrent and optimized via metaheuristic algorithms [6] and due to this kind of methodologies analyses many robot configurations and their performance, the mathematical description must be computationally efficient. From the point of view of their control, the dynamic analysis allows the description in state variables which let to implement robust control strategies. In addition, it allows modeling to be performed at a higher quality level than kinematic modeling because it considers mass inertia characteristics [7]. However, one of the challenges with regards to working with this type of mechanism is that the configuration of closed kinematic chains generates movement restrictions and dependence of all joints, which hinders this type of analysis.

There are different ways to obtain a mathematical model of the dynamics of a parallel robot, such as the Newton–Euler method, Euler–Lagrange method, and the principle of virtual work. The Newton–Euler method is based on Newton's mechanics. One seeks to obtain a dynamic equation that describes the entire mechanism using algebraic operations of the force equations of each link of the robot [8]; however, the description of all forces reactions in control demands is not necessary and requires extra calculation.

On the other hand, the Euler–Lagrange method is based on energies from a global coordinate plane and employs algebra to obtain the dynamic equation [9], but it needs partial derivatives which in optimization strategies must be written on symbolic expressions. These expressions on parallel robots with more than two DoFs are bulky and computationally expensive.

Manuscript received August 29, 2024; revised September 23, 2024; accepted February 7, 2025; published April 14, 2025.

Finally, the virtual work adopts D'Alembert's principle in which the sum of the forces through a virtual displacement of the mechanism is equal to zero. It neither uses partial derivatives nor internal reactions, therefore, it requires the smallest computation time and it can be applied in optimization procedures and real time control strategies [10].

There are studies focused on Hexa manipulator performance, for instance Huynh *et al.* [11] controlled the position of the manipulator via image processing, which includes kinematic modeling but omits dynamics, as the researchers used artificial vision to control the position of the moving platform.

Further, Meng *et al.* [12] presented a novel Hexa robot with three identical limbs designed for high-speed operations. Compared to the classic 6-DOF counterpart used in existing high-speed operations, this newly proposed parallel robot offers a simpler forward displacement model, a larger position workspace, and greater rotational capability. These features make it a promising candidate for applications in high-speed assembly and spatial pick-and-place operations. However, further development is needed, including detailed design refinements and prototype development, to conduct workspace tests and dynamic performance analysis.

Likewise, Hoang *et al.* [13] worked with a Hexa parallel robot and obstacle collision detection method based on a computer vision system but they did not consider a control strategy associated with the movements.

Since there is no evidence of a methodology to solve the inverse dynamics of a parallel Hexa-type robot focused on optimization design and torque control strategy in real time, which also needs to be computationally efficient, this work presents a methodology based on the principle of virtual work for implementation in mathematical software

The remainder of this article is organized as follows. Section II describes the mechanism. Section III presents the position analysis. Section IV presents the velocity analysis. Section V discusses acceleration behavior. Section VI describes the dynamic analysis, and Section VII provides the in-silico validation. The results are presented in Section VIII. Finally, the article concludes in Section IX.

II. Description of Mechanism

A schematic of Hexa is shown in Fig. 1. It consists of six arms with three types of joints: Rotational, Universal, and Spherical (RUS). Each arm was fixed to a base platform by its rotational joint, and, at the other end, the spherical joint was attached to a moving platform. The rotational joint was active because the motors were fixed. In addition, each arm consisted of two links: upper and lower. The former extended from point A to B with length l_b; the latter extended from point B to C with a length l_r; all six arms had the same l_b and l_r values. The i^{th} coordinate of the upper fixed platform vertices is given by Eqs. (1)–(6), whereas the ith vertex of the moving platform is defined in Eqs. (7)–(12) (all of them are based on Fig. 1 $\mathbf{a_i}$ and $\mathbf{c_i}$ are vectors of the center of the fixed and moving platforms, respectively, at the ith vertex, while d_f and d_m are edge magnitudes of the fixed and moving platforms, respectively. Where $\mathbf{R_{oz}}(\cdot)$ is the matrix rotation around *z*.

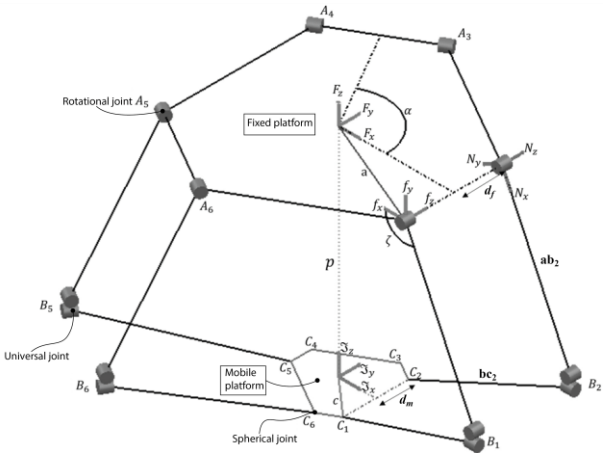

Fig. 1. Schematic of Hexa mechanism-6 RUS.

$$\mathbf{baf}_1 = \left[|\boldsymbol{a}_i|\, cos\left(asin\left(d_f/|\boldsymbol{a}_i|\right)\right) \quad -d_f \quad 0\right]^T \tag{1}$$

$$\mathbf{baf}_2 = \left[|\boldsymbol{a}_i|\, cos\left(asin\left(d_f/|\boldsymbol{a}_i|\right)\right) \quad d_f \quad 0\right]^T \tag{2}$$

$$\mathbf{baf}_3 = \mathbf{R}_{\mathrm{oz}}(120)\,\mathbf{baf}_1 \tag{3}$$

$$\mathbf{baf}_4 = \mathbf{R}_{\mathrm{oz}}(120)\,\mathbf{baf}_2 \tag{4}$$

$$\mathbf{baf}_5 = \mathbf{R}_{\mathrm{oz}}(120)\,\mathbf{baf}_3 \tag{5}$$

$$\mathbf{baf}_6 = \mathbf{R}_{\mathrm{oz}}(120)\,\mathbf{baf}_4 \tag{6}$$

$$\mathbf{pl}_1 = \left[|\boldsymbol{c}_i|\, cos\left(asin(d_m/|\boldsymbol{c}_i|)\right) \quad -d_m \quad 0\right]^T \tag{7}$$

$$\mathbf{pl}_2 = \left[|\boldsymbol{c}_i|\, cos\left(asin(d_m/|\boldsymbol{c}_i|)\right) \quad d_m \quad 0\right]^T \tag{8}$$

$$\mathbf{pl}_3 = \mathbf{R}_{\mathrm{oz}}(120^{\mathrm{o}})\,\mathbf{pl}_1 \tag{9}$$

$$\mathbf{pl}_4 = \mathbf{R}_{\mathrm{oz}}(120^{\mathrm{o}})\,\mathbf{pl}_2 \tag{10}$$

$$\mathbf{pl}_5 = \mathbf{R}_{\mathrm{oz}}(120^{\mathrm{o}})\,\mathbf{pl}_3 \tag{11}$$

$$\mathbf{pl}_6 = \mathbf{R}_{\mathrm{oz}}(120^{\mathrm{o}})\,\mathbf{pl}_4 \tag{12}$$

The rotation matrix of the absolute reference *F* to the reference in the center of the moving platform ($\Im$) (Fig. 1) is determined using 3-1-2 Euler angle set (13), where φ, θ, and ψ are the rotation angles, and $\mathbf{R}_{\mathrm{ox}}(\cdot)$ and $\mathbf{R}_{\mathrm{oy}}(\cdot)$ are the rotation matrices around x and y respectively.

$${}^{F}\mathbf{R}_{\Im} = \mathbf{R}_{\mathrm{oy}}(\varphi)\,\mathbf{R}_{\mathrm{ox}}(\theta)\,\mathbf{R}_{\mathrm{oz}}(\psi) \tag{13}$$

III. Position Analysis

The position analysis of the mechanism determines the rotation values of the arms for the desired positions and angles of the moving platform. This procedure is based on the use of rotation matrices as proposed by Nunez *et al.* [14]. Initially, a reference is found relating to each vertex of the fixed platform (Fi) and the moving platform ($\mathcal{F}i$). ${}^{F}\mathbf{R}_{Fi}$ and ${}^{\Im}\mathbf{R}_{\mathcal{F}i}$ represent the rotation matrices from *F* to Fi and from $\Im$ to $\mathcal{F}i$, respectively, and they are expressed in equation (14). This depends on the

angle of rotation α_i expressed in Eq. (15), considering i =1, …, 6.

$$^{F}\mathbf{R}_{Fi} = {}^{\Im}\mathbf{R}_{\mathcal{F}i} = \mathbf{R}_{\mathrm{oz}}(\alpha_i) \tag{14}$$

where,

$$\alpha = [0 \quad 0 \quad 2\pi/3 \quad 2\pi/3 \quad 4\pi/3 \quad 4\pi/3] \tag{15}$$

In Fig. 1, the reference frame f_i, whose components are $x_{fi}, y_{fi}, z_{fi} (f_i = [x_{fi}, y_{fi}, z_{fi}])$, is configured to match z_{fi} with the axis of rotation. In addition, this is performed so that y_{fi} is perpendicular with respect to the fixed platform. Consequently, the rotation of frame f_i from Fi is given by Eq. (16).

$$^{Fi}\mathbf{R}_{fi} = \mathbf{R}_{\mathrm{oz}}(180^o)\, \mathbf{R}_{\mathrm{ox}}(90^o) \tag{16}$$

The vector describing the i^{th} upper link ($\mathbf{ab}_i$) is defined by Eq. (17), which starts at point A_i and ends at B_i; and ζ is the angle of rotation of the active joint, according to Fig. 1.

$$\mathbf{ab}_i = {}^{F}\mathbf{R}_{Fi}\, {}^{Fi}\mathbf{R}_{fi}\, l_b[cos\,(\zeta_i), sin(\zeta_i), 0]^T \tag{17}$$

The position of the universal joint B_i from reference F ($\mathbf{pb}_i$) is defined in Eq. (18), and the position of point A_i from reference F is $\mathbf{pa}_i$.

$$\mathbf{pb}_i = \mathbf{ab}_i + \mathbf{pa}_i \tag{18}$$

Considering that the desired position of the moving platform ($\mathbf{p}$) is given by Eq. (19). The position of spherical joint C_i from reference F ($\mathbf{pc}_i$) is defined in Eq. (20).

$$\mathbf{p} = [x \quad y \quad z] \tag{19}$$

$$\mathbf{pc}_i = {}^{F}\mathbf{R}_{\Im}\, {}^{\Im}\mathbf{R}_{\mathcal{F}i}\, \mathbf{pl}_i + \mathbf{p}^{\mathrm{T}} \tag{20}$$

If $\mathbf{pb}_i = [pb_{xi} \quad pb_{yi} \quad pb_{zi}]^T$ and $\mathbf{pc}_i = [pc_{xi} \quad pc_{yi} \quad pc_{zi}]^T$, then the squared length of link ${l_r}^2$ corresponds to Eq. (21).

$$\begin{aligned} {l_r}^2 &= (pc_{xi} - pb_{xi})^2 + \left(pc_{yi} - pb_{yi}\right)^2 \\ &\quad + (pc_{zi} - pb_{zi})^2 \\ 0 &= (pc_{xi} - pb_{xi})^2 + \left(pc_{yi} - pb_{yi}\right)^2 \\ &\quad + (pc_{zi} - pb_{zi})^2 - {l_{ri}}^2 \end{aligned} \tag{21}$$

Eq. (21) can be expressed as the product of two vectors equal to zero, as indicated by Eq. (22).

$$\mathbf{e}\,[sin^2(\zeta_i) \quad sin(\zeta_i) \quad cos^2(\zeta_i) \quad cos(\zeta_i) \quad 1]^T = 0 \tag{22}$$

where,

$$\mathbf{e} = [e_{1i} \quad e_{2i} \quad e_{3i} \quad e_{4i} \quad e_{5i}]$$

Therefore, ζ_i is defined by Eq. (23):

$$\zeta_i = arctan(num/den) \tag{23}$$

where,

$$e_{15i} = e_{1i} + e_{5i}$$

$$num = \left\{e_{15i}{e_{2i}}^2 - e_{4i}[-{e_{2i}}^2({e_{15i}}^2 - {e_{4i}}^2 - {e_{2i}}^2)]^{1/2}\right\}[e_{2i}({e_{4i}}^2 + {e_{2i}}^2)]^{-1}$$

$$den = \left\{e_{15i}{e_{4i}}^2 + e_{4i}[-{e_{2i}}^2({e_{15i}}^2 - {e_{4i}}^2 - {e_{2i}}^2)]^{1/2}\right\}({e_{4i}}^2 + {e_{2i}}^2)^{-1}$$

At point A_i there is a reference frame $N_i = [x_{Ni}, y_{Ni}, z_{Ni}]$, the z_{Ni} axis coincides with z_{fi} as Eq. (16), and x_{Ni} with direction of $\mathbf{ab}_i$. Consequently, the rotation of frame N_i from f_i is given by Eq. (24).

$$^{fi}\mathbf{R}_{Ni} = \mathbf{R}_{\mathrm{oz}}(\zeta_i) \tag{24}$$

After considering Eqs. (14), (16), and (24), the rotation of reference frame N_i from F is given by Eq. (25):

$$^{F}\mathbf{R}_{Ni} = {}^{F}\mathbf{R}_{Fi}\, {}^{Fi}\mathbf{R}_{fi}\, {}^{fi}\mathbf{R}_{Ni} \tag{25}$$

It is necessary to determine the unit vector $\mathbf{q}_i$, which has the same direction as the link that points to C_i from B_i. The first step is to determine the equation of the closed chain of each limb according to Eq. (26), where $\mathbf{s}_i$ is the unit vector expressed in Eq. (27) which points to B_i from A_i.

$$\mathbf{pa}_i + l_b\mathbf{s}_i + l_r\mathbf{q}_i = \mathbf{pc}_i \tag{26}$$

$$\mathbf{s}_i = {}^{F}\mathbf{R}_{Ni}\,(|[l_b \quad 0 \quad 0]|^{-1}[l_b \quad 0 \quad 0]^T) \tag{27}$$

Therefore, $\mathbf{q}_i$ is given by Eq. (28):

$$\mathbf{q}_i = {l_r}^{-1}(\mathbf{pc}_i - \mathbf{pa}_i - l_b\mathbf{s}_i) \tag{28}$$

Now, it is necessary to determine the rotation angles of the universal joint (μ_{1i} and μ_{2i}), which rotate the frame $h_i = [x_{\mathrm{h}i}, y_{\mathrm{h}i}, z_{\mathrm{h}i}]$ from the reference F ($^{F}\mathbf{R}_{hi}$). Considering that the x_{hi} axis must be aligned with the lower link ($\mathbf{bc}_i$) and the $z_{\mathrm{h}i}$ axis with the lower rotation axis of the universal joint, the first step is to rotate 90^o about the x_{Ni} in reference frame N_i (Fig. 2(a)), which generates a new reference frame Pi , where $^{Ni}\mathbf{R}_{Pi} = \mathbf{R}_{\mathrm{ox}}(90^o)$.

Then, the rotation matrix of the reference h_i from $P_i = [x_{\mathrm{P}i}, y_{\mathrm{P}i}, z_{\mathrm{P}i}]$ can be calculated. Initially, the $x_{\mathrm{P}i}$ axis is aligned with $\mathbf{ab}_i$; thus, a first rotation μ_{1i} must be made from the $y_{\mathrm{P}i}$ axis. Then, angle μ_{2i} is rotated on the z-axis of the new reference, as defined in Eq. (29) (Fig. 2(b)).

$$^{Pi}\mathbf{R}_{hi} = {}^{Ni}\mathbf{R}_{Pi}\mathbf{R}_{\mathrm{oy}}(hu_{1i})\, \mathbf{R}_{\mathrm{oz}}(hu_{2i}) \tag{29}$$

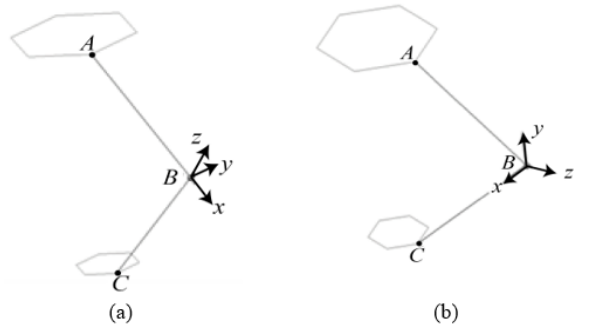

Fig. 2. Location of reference planes: (a) *P* and (b) *h*.

Thus, ${}^{F}\mathbf{R}_{hi}$ is given by Eq. (30), as shown in Fig. 2(b). ${}^{F}\mathbf{R}_{hi}$ is relevant for determining the internal forces of lower links, which is detailed in Section VI.B.

$$ {}^{F}\mathbf{R}_{hi} = {}^{F}\mathbf{R}_{Ni}{}^{Ni}\mathbf{R}_{Pi}{}^{Pi}\mathbf{R}_{hi} \tag{30} $$

Angles μ_{1i} and μ_{2i} are determined as follows. If vector $\mathbf{q}_i$ from hi is given by Eq. (31), and $\mathbf{q}_i$ from F is given by Eq. (28), $\mathbf{q}_i$ is then defined using Eq. (32), where $\mathbf{Qa}_i$ is the transformation matrix.

$$ {}^{hi}\mathbf{q}_i = [1 \quad 0 \quad 0]^{\mathrm{T}} \tag{31} $$

$$ \mathbf{q}_i = {}^{F}\mathbf{R}_{hi}{}^{hi}\mathbf{q}_i = \mathbf{Qa}_i \begin{bmatrix} sin(\mu_{2i}) \\ cos(\mu_{2i})sin(\mu_{1i}) \\ cos(\mu_{2i})cos(\mu_{1i}) \end{bmatrix} \tag{32} $$

where,

$$ \mathbf{Qa}_i = \begin{bmatrix} -cos(\alpha_i)sin(\zeta_i) & -sin(\alpha_i) & -cos(\alpha_i)cos(\zeta_i) \\ -sin(\alpha_i)sin(\zeta_i) & cos(\alpha_i) & -sin(\alpha_i)cos(\zeta_i) \\ -cos(\zeta_i) & 0 & sin(\zeta_i) \end{bmatrix} $$

After inverting matrix $\mathbf{Qa}_i$ and multiplying it by $\mathbf{q}_i$, one can already determine μ_{1i} and μ_{2i} using Eq. (33), considering that $\mathbf{ha}_i = [ha_{1i}, ha_{2i}, ha_{3i}]^{\mathrm{T}}$.

$$ \begin{gathered} \mathbf{Qa}^{-1}\mathbf{q}_i = \mathbf{ha}_i \\ \mu_{1i} = \operatorname{atan}(ha_{2i}/ha_{3i}) \\ \mu_{2i} = \arcsin(ha_{1i}) \end{gathered} \tag{33} $$

Finally, considering Fig. 1, the vector $\mathbf{bc}_i$ is defined by Eq. (34).

$$ \mathbf{bc}_i = \mathbf{pc}_i - (\mathbf{ab}_i + \mathbf{pa}_i) \tag{34} $$

IV. Velocity Analysis

Given that a complete understanding of the system is required, velocity analysis of the system components is likewise required. Initially, the desired linear velocity of the moving platform according to plane *F* is given in Eq. (35) and the angular velocity of the moving platform according to the rotation (13) is given by Eq. (36).

$$ \mathbf{v}_p = [\dot{x} \quad \dot{y} \quad \dot{z}] \tag{35} $$

$$ \mathbf{w}_p = \begin{bmatrix} \dot{\psi}\,cos(\varphi) + \dot{\theta}\,sin(\varphi)\,cos\,(\psi) \\ -\dot{\psi}\,sin(\varphi) + \dot{\theta}cos\,(\psi)cos\,(\varphi) \\ -\dot{\theta}\,sin(\psi) + \dot{\varphi} \end{bmatrix}^{\mathrm{T}} \tag{36} $$

If the rotation of the i^{th} upper link regarding fi is ζ_i, the angular velocity concerning fi is then described as $\dot{\zeta}_i$. With respect to reference plane *F*, the angular velocity of the joint is $\dot{\boldsymbol{\xi}}_i$ and is given by Eq. (37).

$$ \dot{\boldsymbol{\xi}}_i = {}^{F}\mathbf{R}_{Fi}{}^{Fi}\mathbf{R}_{fi}\,[0 \quad 0 \quad \dot{\zeta}_i]^{\mathrm{T}} \tag{37} $$

The linear velocity of the center of mass of the upper link is given by Eq. (38).

$$ \mathbf{v}_{bi} = \dot{\boldsymbol{\xi}}_i \times (0.5\mathbf{ab}_i) \tag{38} $$

Spherical joint velocity $\dot{\mathbf{pc}}_i$ is given by Eq. (39).

$$ \dot{\mathbf{pc}}_i = \mathbf{v}_p + \mathbf{w}_p \times (\mathbf{pc}_i - \mathbf{p}^{\mathrm{T}}) \tag{39} $$

On the other hand, $\dot{\mathbf{pc}}_i$ can be expressed as Eq. (40), where $\dot{\mathbf{pb}}_i$ is the velocity of $\mathbf{pb}_i$ and $\mathbf{wr}_i$ is the angular velocity of the i^{th} lower link.

$$ \dot{\mathbf{pc}}_i = \dot{\mathbf{pb}}_i + \mathbf{wr}_i \times \mathbf{bc}_i \tag{40} $$

Furthermore, velocity $\dot{\mathbf{pb}}_i$ according to Eq. (40) is Eq. (41).

$$ \dot{\mathbf{pb}}_i = \dot{\mathbf{pc}}_i - \mathbf{wr}_i \times \mathbf{bc}_i \tag{41} $$

Eq. (46) can also be described as Eq. (42).

$$ \dot{\mathbf{pb}}_i = \dot{\boldsymbol{\xi}}_i \times \mathbf{ab}_i \tag{42} $$

After combining Eqs. (39)–(42), one obtains Eq. (43).

$$ \begin{aligned} \mathbf{wr}_i \times \mathbf{bc}_i = \mathbf{v_p} + \mathbf{w_p} \times (\mathbf{pc}_i - \mathbf{p}^{\mathrm{T}}) \\ - \dot{\boldsymbol{\xi}}_i \times \mathbf{ab}_i \end{aligned} \tag{43} $$

To obtain $\mathbf{wr}_i$, both sides of Eq. (43) are multiplied by the cross-product of $\mathbf{bc}_i$ and then divided by the negative square norm of $\mathbf{bc}_i$, as shown in Eq. (44).

$$ \begin{aligned} \mathbf{wr}_i = -|\mathbf{bc}_i|^{-2}\big[\big(\mathbf{v_p} + \mathbf{w_p} \times (\mathbf{pc}_i - \mathbf{p}^{\mathrm{T}}) \\ - \dot{\boldsymbol{\xi}}_i \times \mathbf{ab}_i\big) \times \mathbf{bc}_i\big] \end{aligned} \tag{44} $$

V. Acceleration Analysis

The desired linear acceleration of the moving platform according to plane *F* is given by Eq. (45) and its angular acceleration is expressed as Eq. (46), where $c(\cdot)$ and $s(\cdot)$ represent cosine and sine, respectively.

$$\dot{\mathbf{v}}_p = [\ddot{x} \quad \ddot{y} \quad \ddot{z}] \tag{45}$$

$$\dot{\mathbf{w}}_p = \begin{bmatrix} c(\varphi)\ddot{\psi} + c(\psi)s(\varphi)\ddot{\theta} - s(\varphi)\dot{\varphi}\dot{\psi} + c(\psi)c(\varphi)\dot{\varphi}\dot{\theta} - s(\psi)s(\varphi)\dot{\theta}\dot{\psi} \\ c(\psi)c(\varphi)\ddot{\theta} - s(\varphi)\ddot{\psi} - c(\varphi)\dot{\psi}\dot{\varphi} - c(\varphi)s(\dot{\psi})\dot{\psi}\dot{\theta} - c(\psi)s(\varphi)\dot{\theta}\dot{\varphi} \\ \ddot{\varphi} - c(\psi)\dot{\psi}\dot{\theta} - s(\psi)\ddot{\theta} \end{bmatrix}^{\mathrm{T}} \tag{46}$$

The acceleration of the moving platform is related to the angular acceleration of the rotational joint. For this reason, from Eq. (37), we obtain Eq. (47), where $\ddot{\zeta}_\iota$ is the angular acceleration of the active joint, and $\ddot{\boldsymbol{\xi}}_\iota = [\ddot{\xi}_{xi} \quad \ddot{\xi}_{yi} \quad \ddot{\xi}_{zi}]$ are the three components of the vector resulting from the rotations with respect to reference frame *F*.

$$\begin{aligned} \ddot{\boldsymbol{\xi}}_\iota = {}^{F}\mathbf{R}_{Fi}\,{}^{Fi}\mathbf{R}_{fi}\,[0 \quad 0 \quad \ddot{\zeta}_\iota]^{\mathrm{T}} \\ = [\ddot{\xi}_{xi} \quad \ddot{\xi}_{yi} \quad \ddot{\xi}_{zi}]^{\mathrm{T}} \end{aligned} \tag{47}$$

The linear acceleration of the i^{th} upper link center of mass is calculated by deriving Eq. (38), which generates Eq. (48).

$$\dot{\mathbf{v}}_{\mathbf{b}i} = \ddot{\boldsymbol{\xi}}_\iota \times (0.5\mathbf{ab}_i) + \dot{\boldsymbol{\xi}}_i \times \left(\dot{\boldsymbol{\xi}}_i \times (0.5\mathbf{ab}_i)\right) \tag{48}$$

By deriving Eq. (43) and considering Eq. (47), the acceleration of the mechanism can be described as in Eq. (49), where the angular acceleration of the i^{th} lower link is $\dot{\mathbf{wr}}_i$.

$$\dot{\mathbf{wr}}_\iota \times \mathbf{bc}_i = \dot{\mathbf{wr}}\mathbf{1}_i + \dot{\mathbf{wr}}\mathbf{2}_i + \dot{\mathbf{wr}}\mathbf{3}_i \tag{49}$$

Here,

$$\begin{aligned} \dot{\mathbf{wr}}\mathbf{1}_i &= \dot{\mathbf{v}}_\mathbf{p} + \dot{\mathbf{w}}_\mathbf{p} \times (\mathbf{pc}_i - \mathbf{p}^{\mathrm{T}}) \\ \dot{\mathbf{wr}}\mathbf{2}_i &= \mathbf{w}_\mathbf{p} \times \left(\mathbf{w}_\mathbf{p} \times (\mathbf{pc}_i - \mathbf{p}^{\mathrm{T}})\right) - \ddot{\boldsymbol{\xi}}_\iota \times \mathbf{ab}_i \\ &\quad - \mathbf{wr}_i \times (\mathbf{wr}_i \times \mathbf{bc}_i) \\ \dot{\mathbf{wr}}\mathbf{3}_i &= \dot{\boldsymbol{\xi}}_i \times \left(\dot{\boldsymbol{\xi}}_i \times \mathbf{ab}_i\right) \end{aligned}$$

A. Velocity Jacobian Matrix

A critical step in formulating the equations of motion is the determination of Jacobian matrices (**Jp**), which express the relationship between the velocity of the joints ($\dot{\boldsymbol{\Phi}}$) and the velocity of moving platform $\dot{\mathbf{xp}}$, where $\dot{\mathbf{xp}} = [\dot{x} \quad \dot{y} \quad \dot{z} \quad \dot{\theta} \quad \dot{\varphi} \quad \dot{\psi}]$, as described in equation (50).

$$\dot{\boldsymbol{\Phi}} = \mathbf{Jp}\,\dot{\mathbf{xp}} \tag{50}$$

With regards to the manipulator, Eq. (48) describes the velocity of the system. To obtain the Jacobian matrix, it is necessary to determine $\dot{\zeta}_\iota$. Thus, the expression to the left of Eq. (43) is eliminated using the dot product, as shown in Eq. (51).

$$\begin{aligned} (\mathbf{wr}_i \times \mathbf{bc}_i) \cdot \mathbf{bc}_i = 0 \\ = \left(\mathbf{v}_\mathbf{p} + \mathbf{w}_\mathbf{p} \times (\mathbf{pc}_i - \mathbf{p}^{\mathrm{T}})\right. \\ \left. - \dot{\boldsymbol{\xi}}_\iota \times \mathbf{ab}_i\right) \cdot \mathbf{bc}_i \end{aligned} \tag{51}$$

The right side of Eq. (51) can be expressed as the multiplication of two vectors, where term $\dot{\zeta}_\iota$ can be factored, as indicated in Eq. (52).

$$0 = \mathbf{u}_i \begin{bmatrix} \dot{\zeta}_\iota & \mathbf{v}_p & \mathbf{w}_p \end{bmatrix}^{\mathrm{T}} \tag{52}$$

where,

$$\mathbf{u}_i = [u_{1i} \quad u_{2i} \quad u_{2i} \quad u_{3i} \quad u_{4i} \quad u_{5i} \quad u_{6i} \quad u_{7i}]$$

Thus, $\dot{\zeta}_\iota$ is given by Eq. (53), where $\mathbf{Jp_i}$ is the ith row of the Jacobian matrix.

$$\begin{aligned} \dot{\zeta}_\iota &= -u_{1i}{}^{-1}[u_{2i} \quad u_{3i} \quad u_{4i} \quad u_{5i} \quad u_{6i} \quad u_{7i}] \quad [\mathbf{v}_p \quad \mathbf{w}_p]^{\mathrm{T}} \\ \dot{\zeta}_\iota &= \mathbf{Jp}_i \quad [\mathbf{v}_p \quad \mathbf{w}_p]^{\mathrm{T}} \end{aligned} \tag{53}$$

B. Acceleration Jacobian Matrix

Another fundamental step is the determination of the transformation of the acceleration of the moving platform ($\ddot{\mathbf{xp}}$) to the acceleration of the active joints ($\ddot{\boldsymbol{\Phi}}$) [15]. This is described by Eq. (54), where **Ja1** is a 6×6 matrix and **Ja2** is a 6×1 vector.

$$\ddot{\boldsymbol{\Phi}} = \mathbf{Ja1}\,\ddot{\mathbf{xp}} + \mathbf{Ja2} \tag{54}$$

The basis of this transformation is Eq. (49). To operate the right side of the expression, the dot product is used, which results in Eq. (55).

$$\begin{aligned} (\dot{\mathbf{wr}}_\iota \times \mathbf{bc}_i) \cdot \mathbf{bc}_i = 0 \\ = \left(\dot{\mathbf{wr}}\mathbf{1}_i + \dot{\mathbf{wr}}\mathbf{2}_i\right. \\ \left. + \dot{\mathbf{wr}}\mathbf{3}_i\right) \cdot \mathbf{bc}_i \end{aligned} \tag{55}$$

The right side of Eq. (55) can be expressed as the multiplication of two vectors, where the angular acceleration of active joint $\ddot{\zeta}_\iota$ can be factored in Eq. (56).

$$0 = \mathbf{r}_i \begin{bmatrix} \ddot{\zeta}_\iota & \dot{\mathbf{v}}_p & \dot{\mathbf{w}}_p & 1 \end{bmatrix}^{\mathrm{T}} \tag{56}$$

where,

$$\mathbf{r}_i = [r_{1i} \quad r_{2i} \quad r_{3i} \quad r_{4i} \quad r_{5i} \quad r_{6i} \quad r_{7i} \quad r_{8i}]$$

Thus, $\ddot{\zeta}_\iota$ can be formulated as Eq. (54), where $\mathbf{Ja1}_i$ and $Ja2_i$ correspond to the ith row of the transformation, as illustrated in Eq. (57).

$$\begin{aligned} \mathbf{Ja1}_i &= -r_{1i}{}^{-1}[r_{2i} \quad r_{3i} \quad r_{4i} \quad r_{5i} \quad r_{6i} \quad r_{7i}] \\ Ja2_i &= -r_{1i}{}^{-1} r_{8i} \\ \ddot{\zeta}_\iota &= \mathbf{Ja1}_i\,[\dot{\mathbf{v}}_p \quad \dot{\mathbf{w}}_p]^{\mathrm{T}} + Ja2_i \end{aligned} \tag{57}$$

C. Link Jacobian Matrix

The angular velocity of the active joint relative to the reference frame fi ($^{fi}\boldsymbol{\vartheta}$) can be expressed as a 6×3 matrix, according to Eq. (58), where $\mathbf{0}_{6\,X\,2}$ is a matrix of 6×2 zeros.

$$^{fi}\dot{\boldsymbol{\vartheta}}_i = [\mathbf{0}_{6x2} \quad \mathbf{Jp}\,\dot{\mathbf{xp}}^{\mathrm{T}}] \tag{58}$$

The velocity of the center of mass of the ith upper link with reference F $\left(\dot{\mathbf{Rb}}_i\right)$ is formulated as Eq. (59).

$$\dot{\mathbf{Rb}}_i = \left({}^{F}\mathbf{R}_{Fi}\;{}^{Fi}\mathbf{R}_{fi}\;{}^{fi}\dot{\boldsymbol{\vartheta}}_i\right) \times 0.5\mathbf{ab}_i \tag{59}$$

Therefore, Eq. (59) can be expressed in terms of $\dot{\mathbf{xp}}$, as shown in Eq. (60).

$$\dot{\mathbf{Rb}}_i = \mathbf{JRb}_i\,\dot{\mathbf{xp}} = \begin{bmatrix}\mathbf{JRbx}_i \ldots\\ \mathbf{JRby}_i \ldots\\ \mathbf{JRbz}_i \ldots\end{bmatrix}\dot{\mathbf{xp}} \tag{60}$$

The angular velocity of the i^{th} upper link with respect to F ($\mathbf{wb}_i$) is determined by Eq. (61).

$$\mathbf{wb}_i = {}^{F}\mathbf{R}_{Fi}\;{}^{Fi}\mathbf{R}_{fi}\,[0 \quad 0 \quad \mathbf{Jp}_i\,\dot{\mathbf{xp}}^{\mathrm{T}}] \tag{61}$$

For the velocities of the i^{th} lower link, the angular velocity of the joint was initially calculated in B_i according to Eq. (62), where $\dot{\mathbf{xp}}_{xyz} = [\dot{x} \quad \dot{y} \quad \dot{z}]$ and $\dot{\mathbf{xp}}_{\theta\varphi\psi} = [\dot{\theta} \quad \dot{\varphi} \quad \dot{\psi}]$.

$$\begin{aligned}\mathbf{wr}_i = -|\mathbf{bc}_i|^{-2}\big[&\big(\dot{\mathbf{xp}}_{xyz}\\ &+ \dot{\mathbf{xp}}_{\theta\varphi\psi} \times (\mathbf{pc}_i - \mathbf{p}^{\mathrm{T}})\\ &- \mathbf{wb}_i \times \mathbf{ab}_i\big) \times \mathbf{bc}_i\big]\end{aligned} \tag{62}$$

The linear velocity of the center of mass of the i^{th} lower link is given by Eq. (63).

$$\dot{\mathbf{Rr}}_i = \mathbf{wr}_i \times 0.5\;\mathbf{bc}_i \tag{63}$$

Similarly to Eq. (60), the Jacobian matrices related to $\mathbf{wb}_i$, $\mathbf{wr}_i$, and $\dot{\mathbf{Rr}}_i$ are expressed as Eqs. (64)–(66), respectively.

$$\mathbf{wb}_i = \mathbf{J\omega b}_i\,\dot{\mathbf{xp}} \tag{64}$$

$$\mathbf{wr}_i = \mathbf{J\omega r}_i\,\dot{\mathbf{xp}} \tag{65}$$

$$\dot{\mathbf{Rr}}_i = \mathbf{JRr}_i\,\dot{\mathbf{xp}} = \begin{bmatrix}\mathbf{JRrx}_i \ldots\\ \mathbf{JRry}_i \ldots\\ \mathbf{JRrz}_i \ldots\end{bmatrix}\dot{\mathbf{xp}} \tag{66}$$

VI. Dynamics Analysis

To analyze the inverse dynamics, a desired moving platform trajectory is necessary to determine the torque required in producing the given movement. This depends on the structural parameters, position, kinematics, gravity, external forces, and moment exerted on the movable platform. Therefore, the explicit equation of the mechanism dynamics is Eq. (67), where $\boldsymbol{\tau}$ is the torque vector of the active joints, $\mathbf{M}$ is the inertia matrix, $\mathbf{C}$ is the Coriolis and centrifugal forces, and $\mathbf{ge}$ is the vector of the gravitational forces.

$$\boldsymbol{\tau} = \mathbf{M}\,\ddot{\mathbf{xp}} + \mathbf{C} + \mathbf{ge} \tag{67}$$

The dynamic equations of motion are formulated under the principles of D'Alembert and virtual work because of the aforementioned computational advantages. These equations are formulated using the concept of equipollent forces [16].

The virtual work of the mechanism is related to the work exerted by the moments and forces. The virtual work exerted by the moment is defined as the product of the sum of the moments of the center of mass $\left(Mo^i - J^i\ddot{\theta}^i\right)$, where Mo denotes the moments applied, J denotes the moments of inertia, and $\ddot{\theta}$ represents the angular accelerations and virtual changes in the angular orientation of the body ($\delta\theta^i$). The virtual work exerted by the forces is the product of the resulting forces applied at the center of mass ($\mathbf{F}^i - m^i\mathbf{a}^i$), where $\mathbf{F}$ denotes the forces applied at the center of mass, m is the system mass, and $\mathbf{a}$ represents accelerations due to virtual changes in displacement ($\boldsymbol{\delta}\mathbf{R}^i$) [16], as presented in Eq. (68).

$$\left.\begin{aligned}(\mathbf{F}^i - m^i\mathbf{a}^i)^{\mathrm{T}}\boldsymbol{\delta}\mathbf{R}^i = 0\\ \left(Mo^i - J^i\ddot{\theta}^i\right)\delta\theta^i = 0\end{aligned}\right\} \tag{68}$$

After adding Eqs. (68) and (69), one expresses and classifies the virtual work in two aspects: one generated by external forces (δW_e) and the other caused by internal forces and inertia (δW_i). The internal forces or constraint forces are the reaction forces that arise as the result of the connectivity between different bodies in multibody systems [14].

$$\delta W_e \quad - \quad \delta W_i \quad = 0 \tag{69}$$

where

$$\delta W_e = \mathbf{F}^{i^{\mathrm{T}}}\boldsymbol{\delta}\mathbf{R}^i + Mo^i\delta\theta^i$$

$$\delta W_i = m^i\mathbf{a}^{i^{\mathrm{T}}}\boldsymbol{\delta}\mathbf{R}^i + J^i\ddot{\theta}^i\delta\theta^i$$

As previously described, δW_e relates the external forces ($\mathbf{F_e}$) and δW_i relates to the internal forces ($\mathbf{F_i}$), both of which are associated with an independent coordinate system (δq) according to the study by Shabana [16]. Therefore, Eq. (69) can be expressed as Eq. (70).

$$\begin{aligned}\mathbf{F}_e{}^{\mathrm{T}}\delta q - \mathbf{F}_i{}^{\mathrm{T}}\delta q &= 0\\ \left(\mathbf{F}_{\mathrm{e}}{}^{\mathrm{T}} - \mathbf{F}_i{}^{\mathrm{T}}\right)\delta q &= 0\end{aligned} \tag{70}$$

Since $\delta q \neq 0$, Eq. (71) is obtained.

$$\mathbf{F}_{\mathrm{e}} = \mathbf{F}_i \tag{71}$$

Based on the above, the application of the virtual work principle in the mechanism can focus on external and inertial forces.

A. Determination of Virtual Work of External Forces

The virtual work exerted by external forces on the system is described by Eq. (72), where $\delta\zeta$ is the virtual rotation of the active actuator, δb_z is the virtual displacement in z of the upper link, g is gravity, δr_z is the virtual displacement in z of the lower link, m_b is the total mass of the top link (Eq. (73)), m_r is the total mass of the lower link (Eq. (74)), δz is the virtual displacement in z of the moving platform, and m_p is the mass of the mobile platform.

$$\begin{aligned} F_e = 0 = \delta\zeta\,\tau &+ \delta b_z(-m_b g) \\ &+ \delta r_z(-m_r g) \\ &+ \delta z\left(-m_p g\right) \end{aligned} \tag{72}$$

$$m_b = m_{ES} + 0.5(m_R + m_U) \tag{73}$$

where m_{ES} denotes the mass of the top link, m_R denotes the mass of the rotational joint coupling, and m_U denotes the mass of the universal joint. Regarding m_r(Eq. (74)), m_{EI} is the lower link mass, m_U is the universal join mass, and m_S is the mass of the spherical joint.

$$\mathrm{m}_r = \mathrm{m}_{EI} + 0.5(\mathrm{m}_U + \mathrm{m}_S) \tag{74}$$

After considering Eqs. (53), (60) and (66), Eq. (72) can be rewritten as Eq. (75), where $\boldsymbol{\delta X} = [\delta x \quad \delta y \quad \delta z \quad \delta\theta \quad \delta\varphi \quad \delta\psi]$.

$$\begin{aligned} 0 = (\mathbf{Jp}\boldsymbol{\delta X})^{\mathrm{T}}\boldsymbol{\tau} &+ (\mathbf{JRbz}\boldsymbol{\delta X})(-\mathrm{m}_b g) \\ &+ (\mathbf{JRrz}\boldsymbol{\delta X})(-\mathrm{m}_r g) \\ &+ \delta z\left(-\mathrm{m}_p g\right) \end{aligned} \tag{75}$$

After rearranging Eq. (75) with respect to δX, Eq. (76) is obtained.

$$\begin{aligned} 0 = \; & \boldsymbol{\delta X}^{\mathrm{T}}\Big(\mathbf{Jp}^{\mathrm{T}}\boldsymbol{\tau} + \mathbf{JRbz}^{\mathrm{T}}(-\mathrm{m}_b g) \\ & + \mathbf{JRrz}^{\mathrm{T}}(-\mathrm{m}_r g) \\ & + [0 \quad 0 \quad 1 \quad 0 \quad 0 \quad 0]^{\mathrm{T}}\left(-\mathrm{m}_p g\right)\Big) \end{aligned} \tag{76}$$

Since $\boldsymbol{\delta X} \neq 0$, Eq. (77) is proposed for estimating $\boldsymbol{\tau}$.

$$\begin{aligned} \boldsymbol{\tau} = \; & {\mathbf{J_p}^{\mathrm{T}}}^{-1}\Big(\mathbf{J_{Rbz}}^{\mathrm{T}}(m_b g) + \mathbf{J_{Rrz}}^{\mathrm{T}}(m_r g) \\ & + [0 \quad 0 \quad 1 \quad 0 \quad 0 \quad 0]^{\mathrm{T}}\left(m_p g\right)\Big) \end{aligned} \tag{77}$$

Therefore, the total external forces $\mathbf{F}_{\mathrm{e}}$ is equal to the sum of the forces involved in the virtual work of each of the six limbs plus those related to the moving platform, resulting in Eq. (78).

$$\mathbf{F}_{\mathrm{e}} = \mathbf{Jp}^{-\mathrm{T}}\mathbf{Q}_{\mathrm{e}} - \boldsymbol{\tau} \tag{78}$$

where

$$\mathbf{Q}_{\mathrm{e}} = \sum_i \left(\mathbf{JRbz}_i{}^{\mathrm{T}}(\mathrm{m}_b g) + \mathbf{JRrz}_i{}^{\mathrm{T}}(\mathrm{m}_r g)\right) + [0 \quad 0 \quad 1 \quad 0 \quad 0 \quad 0]^{\mathrm{T}}(\mathrm{m}_p g)$$

B. Analysis of Virtual Work of internal and Inertial Forces

The virtual work of the inertial forces can be analyzed by each component of the system. In this way, F_b, F_r and F_p relate to the forces of the upper and lower links and the mobile platform, respectively, to obtain Eq. (79).

$$\begin{aligned} 0 &= \delta X\, F_b + \delta X\, F_r + \delta X\, F_p \\ 0 &= \delta X\left(F_b + F_r + F_p\right) \end{aligned} \tag{79}$$

Therefore, the first step is to analyze the internal forces of the moving platform (F_p). The inertia tensor of this component with respect to F is Eq. (80), where I_{pc} is the inertia tensor of the platform, which is typically calculated using Computer-Aided Design (CAD) software in which the mechanism is designed.

$$\mathbf{I}_p = {}^{F}\mathbf{R}_{\Im}\,\mathbf{I}_{pc}\,{}^{F}\mathbf{R}_{\Im}{}^{\mathrm{T}} \tag{80}$$

The representation of F_p is Eq. (81), where m_p is the mass of the platform, and $\mathbf{I_{n\,X\,m}}$ is the identity matrix of n × m dimensionality.

$$\mathbf{F}_p = \mathbf{F}_{pM}\ddot{\mathbf{xp}} + \mathbf{F}_{pC} \tag{81}$$

where

$$\mathbf{F}_{pM} = \begin{bmatrix} m_p\,\mathbf{I}_{3x3} & \mathbf{0}_{3x3} \\ \mathbf{0}_{3x3} & \mathbf{I}_p \end{bmatrix} \qquad \mathbf{F}_{pC} = \begin{bmatrix} \mathbf{0}_{3x1} \\ \mathbf{w}_p \times \mathbf{I}_p\mathbf{w}_p \end{bmatrix}$$

The next step is to analyze the internal forces of the ith upper link ($\mathbf{F}_{bi}$). The inertia tensor of the ith upper link with respect to F is given by Eq. (82), where m_b is the mass of the upper link.

$$\mathbf{I}_{bi} = {}^{F}\mathbf{R}_{Ni}\left(\frac{m_b|\mathbf{ab}_i|^2}{3}\begin{bmatrix} 0 & 0 & 0 \\ 0 & 1 & 0 \\ 0 & 0 & 1 \end{bmatrix}\right){}^{F}\mathbf{R}_{Ni}{}^{\mathrm{T}} \tag{82}$$

Considering the internal forces described in the study by Shabana [16] and the virtual displacements, the virtual work of the i^{th} upper link related to the internal forces is given by Eq. (83).

$$\begin{aligned} \mathbf{F}_{bi} = \; & \boldsymbol{\delta R}_{\mathrm{bi}} m_b \dot{\mathbf{vb}}_i + \boldsymbol{\delta w}_b \mathbf{I}_{bi}\dot{\boldsymbol{\xi}}_i \\ & + \boldsymbol{\delta w}_{bi}\left(\dot{\boldsymbol{\xi}}_i \times \left(\mathbf{I}_{bi}\,\dot{\boldsymbol{\xi}}_i\right)\right) \end{aligned} \tag{83}$$

After combining Eqs. (60) and (64), Eq. (83) can be rewritten as Eq. (84).

$$\begin{aligned} \mathbf{F}_{bi} = \; & (\mathbf{JRb}_i\boldsymbol{\delta X})\, m_b \dot{\mathbf{vb}}_i + (\mathbf{J\omega b}_i\boldsymbol{\delta X})\,\mathbf{I}_b\ddot{\boldsymbol{\xi}}_i \\ & + (\mathbf{J\omega b}_i\boldsymbol{\delta X})\left(\dot{\boldsymbol{\xi}}_i \right. \\ & \left. \times \left(\mathbf{I}_{bi}\,\dot{\boldsymbol{\xi}}_i\right)\right) \end{aligned} \tag{84}$$

Based on Eq. (48), and after rearranging Eq. (84) concerning δX, Eq. (85) is obtained.

$$\mathbf{F}_{bi} = \mathbf{JRb}_i m_b \left(\ddot{\boldsymbol{\xi}}_i \times (0.5\mathbf{ab}_i)\right) + \mathbf{J\omega b}_i \mathbf{I}_{bi} \ddot{\boldsymbol{\xi}}_i + \mathbf{JRb}_i m_b \left(\dot{\boldsymbol{\xi}}_i \times \left(\dot{\boldsymbol{\xi}}_i \times (0.5\mathbf{ab}_i)\right)\right) + \mathbf{J\omega b}_i \left(\dot{\boldsymbol{\xi}}_i \times \left(\mathbf{I}_{bi} \dot{\boldsymbol{\xi}}_i\right)\right) \quad (85)$$

$\ddot{\boldsymbol{\xi}}_i$ is factored such that Eq. (85) is expressed as Eq. (86), where $\mathbf{Y}_i$ is a 6×3 matrix resulting from the factorization of $\ddot{\boldsymbol{\xi}}_i$.

$$\mathbf{F}_{bi} = \mathbf{Y}_i \ddot{\boldsymbol{\xi}}_i + \mathbf{JRb}_i m_b \left(\dot{\boldsymbol{\xi}}_i \times \left(\dot{\boldsymbol{\xi}}_i \times (0.5\mathbf{ab}_i)\right)\right) + \mathbf{J\omega b}_i \left(\dot{\boldsymbol{\xi}}_i \times \left(\mathbf{I}_{bi} \dot{\boldsymbol{\xi}}_i\right)\right) \quad (86)$$

$\mathbf{EC}_i$ is a 6×3 matrix in which each column is represented as $\mathbf{EC}_i = [\mathbf{ec}_{1i} \quad \mathbf{ec}_{2i} \quad \mathbf{ec}_{3i}]$, and $\mathbf{F}_{bi}$ can be expressed as Eq. (87).

$$\mathbf{F_{bi}} = [\mathbf{ec}_{1i} \quad \mathbf{ec}_{2i} \quad \mathbf{ec}_{3i}][0 \quad 0 \quad \mathbf{Ja1}_i \ddot{\mathbf{xp}} + \mathbf{Ja2}_i]^{\mathrm{T}} + \mathbf{JRb}_i m_b \left[\dot{\boldsymbol{\xi}}_i \times \left(\dot{\boldsymbol{\xi}}_i \times (0.5\mathbf{ab}_i)\right)\right] + \mathbf{J\omega b}_i \left(\dot{\boldsymbol{\xi}}_i \times \left(\mathbf{I}_{bi} \dot{\boldsymbol{\xi}}_i\right)\right) \quad (87)$$

where $\mathbf{ec}_i = {}^{F}\mathbf{R}_{Fi}{}^{Fi}\mathbf{R}_{fi}\mathbf{Y}_i$

The representation of $\mathbf{F}_b$ is Eq. (88).

$$\mathbf{F}_b = \mathbf{F}_{bM} \ddot{\mathbf{xp}} + \mathbf{F}_{bC} \quad (88)$$

where

$$\mathbf{F}_{bM} = \sum_i \mathbf{ec}_{3i} \mathbf{Ja1}_i$$

$$\mathbf{F}_{bC} = \sum_i \mathbf{ec}_{3i} \mathbf{Ja2}_i + \sum_i \mathbf{JRb}_i m_b \left(\dot{\boldsymbol{\xi}}_i \times \left(\dot{\boldsymbol{\xi}}_i \times (0.5\mathbf{ab}_i)\right)\right) + \mathbf{J\omega b}_i \left(\dot{\boldsymbol{\xi}}_i \times \left(\mathbf{I}_{bi} \dot{\boldsymbol{\xi}}_i\right)\right)$$

Next, the internal forces of the i^{th} lower link (F_{ri}) are determined. The inertia tensor of the lower link with respect to F is given by Eq. (89), where m_r is the mass of the lower link.

$$\mathbf{I}_{ri} = {}^{F}\mathbf{R}_{hi} \left(\frac{m_r |\mathbf{bc}_i|^2}{3} \begin{bmatrix} 0 & 0 & 0 \\ 0 & 1 & 0 \\ 0 & 0 & 1 \end{bmatrix}\right) {}^{F}\mathbf{R}_{hi}{}^{\mathrm{T}} \quad (89)$$

The virtual work of the ith lower link related to the internal forces is Eq. (90), where δR_r is the virtual displacement of the lower link and δw_r is the virtual rotation of the lower link.

$$\mathbf{F}_{ri} = \delta R_r m_r \dot{\mathbf{vr}} + \delta w_r \mathbf{I}_r \dot{\mathbf{wr}}_i + \delta w_r \left(\mathbf{wr}_i \times (\mathbf{I}_{ri} \mathbf{wr}_i)\right) \quad (90)$$

After considering Eqs. (65) and (66), Eq. (90) can be rewritten as Eq. (91).

$$\mathbf{F}_{ri} = (\mathbf{JRr_i} \delta X) m_r \dot{\mathbf{vr}} + (\mathbf{J\omega r}_i \delta X) \mathbf{I}_r \dot{\mathbf{wr}}_i + (\mathbf{J\omega r}_i \delta X) \left(\mathbf{wr}_i \times (\mathbf{I}_{ri} \mathbf{wr}_i)\right) \quad (91)$$

After rearranging Eq. (91) with respect to δX, F_{ri} is obtained according to Eq. (92), where $\mathbf{O}_i$ corresponds to a 6×3 matrix that represents the factorization of $(\mathbf{JRr}_i m_r)\left(\dot{\mathbf{wr}}_i \times (0.5\mathbf{bc}_i)\right) + (\mathbf{J\omega r}_i \mathbf{I}_{ri})$ with respect to $\dot{\mathbf{wr}}_i$.

$$\mathbf{F}_{ri} = \mathbf{O}_i \dot{\mathbf{wr}}_i + \mathbf{J\omega r}_i{}^{\mathrm{T}} (\mathbf{wr}_i \times \mathbf{I}_{ri} \mathbf{wr}_i) \quad (92)$$

In addition, Eq. (92) can be expressed as Eq. (93), where $\mathbf{Sa}_i$ is a 6×3 matrix denoted as $\mathbf{Sa}_i = {}^{F}\mathbf{R}_{Fi}{}^{Fi}\mathbf{R}_{fi}\mathbf{O}_i$ and each column can be expressed as $\mathbf{Sa}_i = [\mathbf{sa}_{1i} \quad \mathbf{sa}_{2i} \quad \mathbf{sa}_{3i}]$.

$$\mathbf{F}_{ri} = \mathbf{Sa}_i [0 \quad 0 \quad \mathbf{Ja1}_i \ddot{\mathbf{xp}} + \mathbf{Ja2}_i]^{\mathrm{T}} + \mathbf{O}_i (\dot{\mathbf{wr1}}_i + \dot{\mathbf{wr2}}_i) + \mathbf{J\omega r}_i{}^{\mathrm{T}} (\mathbf{wr}_i \times \mathbf{I}_{ri} \mathbf{wr}_i) \quad (93)$$

Therefore, the forces related to the lower link are given in Eq. (94).

$$\mathbf{F}_r = \mathbf{F}_{rM} \ddot{\mathbf{xp}} + \mathbf{F}_{rM} \quad (94)$$

where

$$\mathbf{F}_{rM} = \sum_i (\mathbf{sa}_{3i} \mathbf{Ja1}_i)$$

$$\mathbf{F}_{rC} = \sum_i \mathbf{sa}_{3i} \mathbf{Ja2}_i + \mathbf{O}_i (\dot{\mathbf{wr1}}_i + \dot{\mathbf{wr2}}_i) + \mathbf{J\omega r}_i (\mathbf{wr}_i \times \mathbf{I}_{ri} \mathbf{wr}_i)$$

After combining Eqs. (71), (78), (88), and (94) $\boldsymbol{\tau}$ is determined by Eq. (95).

$$\boldsymbol{\tau} = \mathbf{Jp}^{\mathrm{T}^{-1}} \mathbf{Q}_{\mathrm{e}} - \mathbf{F}_{rM} \ddot{\mathbf{xp}} - \mathbf{F}_{bM} \ddot{\mathbf{xp}} - \mathbf{F}_{bC} - \mathbf{F}_{rM} \quad (95)$$

Finally, the expressions $\mathbf{M}$ in Eq. (96), $\mathbf{C}$ in Eq. (97) and $\mathbf{G}$ in Eq. (98) are defined from Eq. (67).

$$\mathbf{M} = -\mathbf{Jp}^{\mathrm{T}^{-1}} \left(\mathbf{F}_{pM} + \mathbf{F}_{bM} + \mathbf{F}_{rM}\right) \quad (96)$$

$$\mathbf{C} = -\mathbf{Jp}^{\mathrm{T}^{-1}} \left(\mathbf{F}_{pC} + \mathbf{F}_{bC} + \mathbf{F}_{rC}\right) \quad (97)$$

$$\mathbf{ge} = \mathbf{Jp}^{\mathrm{T}^{-1}} \mathbf{Q}_{\mathrm{e}} \quad (98)$$

VII. Validation

This model was validated by comparing the proposed dynamic model to the CAD assembly in the MATLAB multiphysics environment. Fig. 3 shows the structure of the comparison, where $\ddot{X}_d$, $\dot{X}_d$, and X_d are the desired accelerations, velocities, and positions of the moving platform, respectively. These signals are processed in

parallel by equal controllers, where one generates the signal in a multiphysics environment, and the other generates it in the dynamic model. The torques required by each option were analyzed to study the similarity between them. For this purpose, it was necessary to apply a control strategy, simplify and implement the CAD model in the multiphysics environment, and obtain the direct dynamics of the mechanism and compare the results. The steps are explained in detail as follows.

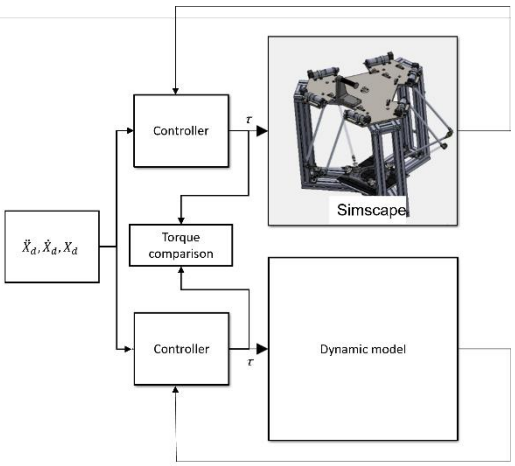

Fig. 3. Torque comparison configuration.

The controller uses a hybrid configuration [14], as indicated in Fig. 4, which considers an equivalent control related to the differential flatness theory [17] delimited in the gray box of Fig. 4, with an attractive strategy-type sliding mode [18] that is located in the black dotted box in Fig. 4. The control signal is the torque that the motors must generate, and the velocity and position of the moving platform are fed back. Thus, the Laplace transform of the error dynamics is performed, and parameters K_v, K_p and K_i are calculated considering the location of the poles according to the damping ratio ξ and undamped natural frequency w_n [19], as shown in Eq. (99).

$$\ddot{e} + K_v\ddot{e} + K_p\dot{e} + K_i e = 0$$

$$s^3 + K_v s^2 + K_p s + K_i = (s^2 + 2\xi w_n s + {w_n}^2)(s + 5\xi w_n) \quad (99)$$

The next step is to simplify the CAD model by removing the screws, Seeger rings, nuts, and other assembly elements to focus on the essentials. The mass of the extracted elements is added to the mass of the corresponding link. This simplified model was imported into a multiphysics environment called Simscape. The position, velocity, and acceleration of the moving platform were extracted to be used as feedback signals.

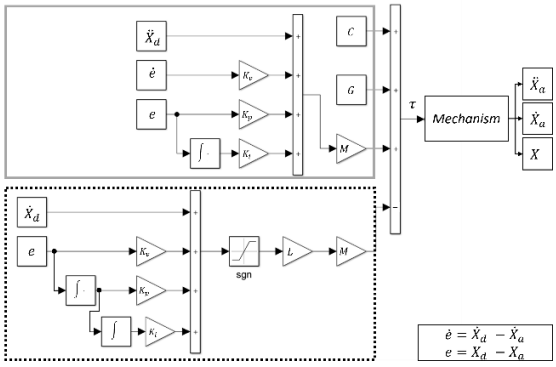

Fig. 4. Schematic of control strategy.

On the other hand, acceleration $\ddot{X}$ of the analytical model is determined considering Eqs. (67), (96), (97) and (98), which results in Eq. (100). This signal is double-integrated to determine the velocity and position of the moving platform.

$$\ddot{\mathbf{xp}} = (\mathbf{M}^{-1}\boldsymbol{\tau}) - (\mathbf{M}^{-1}\mathbf{C}) - (\mathbf{M}^{-1}\mathbf{ge}) \quad (100)$$

Finally, under the same input signals, the signal positions between both models and torque signals are compared. The comparison showed that this symmetrical mechanism, with pairs of actuators in parallel, compensates for their requirements by working together. Fig. 5 indicates that the motors that work in this way are 1-2, 3-4, and 5-6. For this reason, a torque comparison was performed considering this movement.

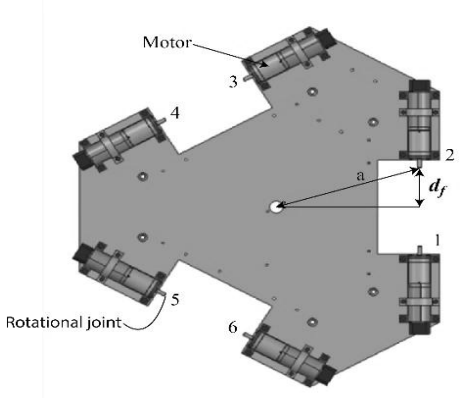

Fig. 5. Fixed platform.

VIII. Results

Table I presents the characteristics of the validated mechanism. The controller constants K_v, K_p, and K_i were calculated considering a settling time of 1 s and ξ of 0.7. These constants are summarized in Table II.

TABLE I. Properties of Mechanism

$\mathbf{m}_R$	$\mathbf{m}_U$	$\mathbf{m}_S$	$\mathbf{m}_{ES}$	$\mathbf{m}_{EI}$	a	D	c	d	l_b	l_r	$\mathbf{m}_p$
(g)	(g)	(g)	(g)	(g)	(mm)	(mm)	(mm)	(mm)	(mm)	(mm)	(g)
168	61	146	80	80	230	89	83.35	60.7	300	300	444

TABLE II. CONTROLLER CONSTANTS VALUES

K_v	K_p	K_i
28 $I_{6\times6}$	192.65 $I_{6\times6}$	653.06 $I_{6\times6}$

Finally, the desired trajectory X_d involving three desired translations and three rotations was proposed and compared with the responses of the analytical model and virtual environment. Fig. 6(a) shows the behavior of the system on the X-axis, where xRef refers to the desired movement, and xDm and xSm refer to the behavior of the analytical and simulated models, respectively. It should be emphasized that both xDm and xSm generated similar behaviors throughout the analysis.

Likewise, the behaviors in the Y-and Z-axes were studied according to Fig. 6(b) and (c), where yRef and zRef refer to the desired movement, and yDm, zDm, ySm, and zSm refer to the behavior of the analytical and simulated models, respectively. In both conditions, the analytical model exhibited similar behavior to Simscape, including overdamped behavior and settling time.

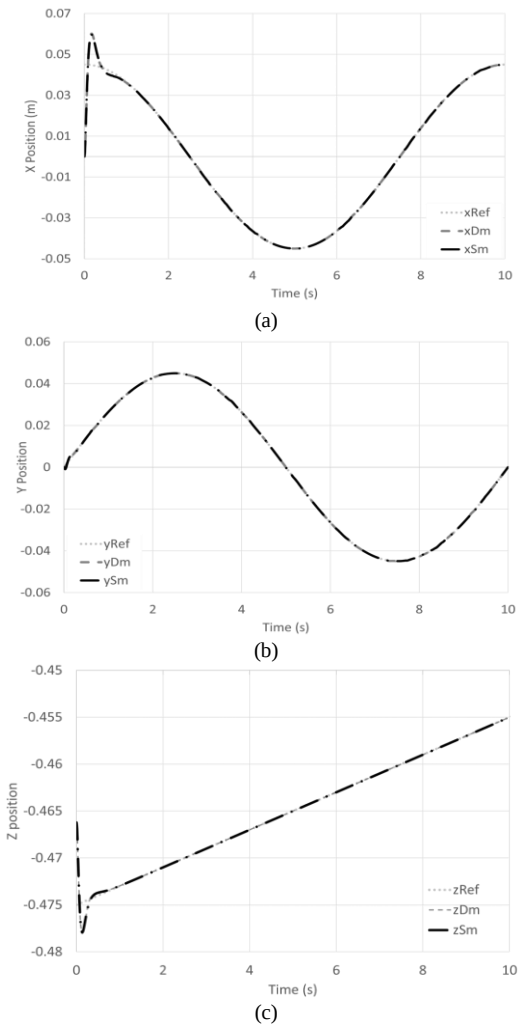

Fig. 6. Comparison between response of analytical model and simulated model at the desired (a) X position. (b) Y position. (c) Z position.

In addition, a comparison was made considering the non-rotation of the moving platform to show the symmetry of the behavior; for this case, the desired rotations of θ, φ and ψ were equal to zero, as represented by aRef, bRef, and eRef in Fig. 7(a), (b), and (c), respectively.

The sum of torques of the actuators of positions 1-2, 3-4, and 5-6 are indicated in Fig. 8 (a), (b) and (c) respectively, where Dt1-2, Dt3-4, and Dt5-6, are obtained by the analytical route and Dt1-2 Sm, Dt3-4 Sm, and Dt5-6 Sm, are obtained by the multiphysics simulation. In the three figures, there are gaps that reach up to 4.5% in some cases. This is caused by approximations and simplifications in the model. The peaks generated in the multiphysics simulation, owing to the torque required for the repositioning of the links following the trajectories, are similar in time and magnitude to those generated by the mathematical model. This implies that the analytical model is also sensitive to these rearrangements.

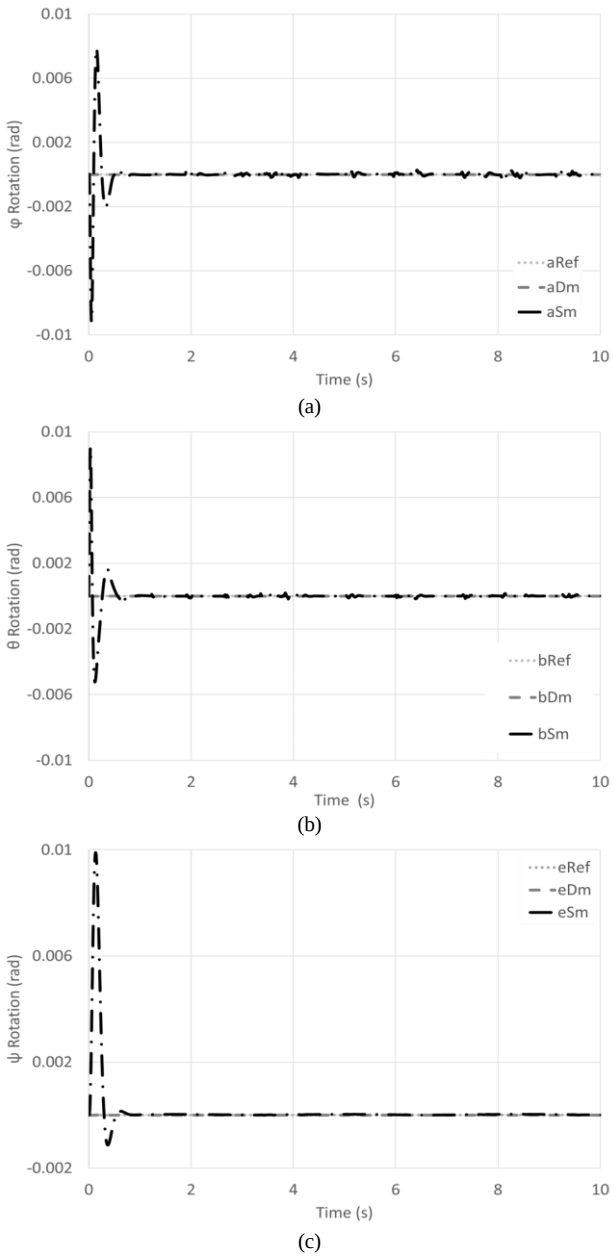

Fig. 7. Comparison between response of analytical model and simulated model at the desired (a) φ rotation. (b) θ rotation. (c) ψ rotation.

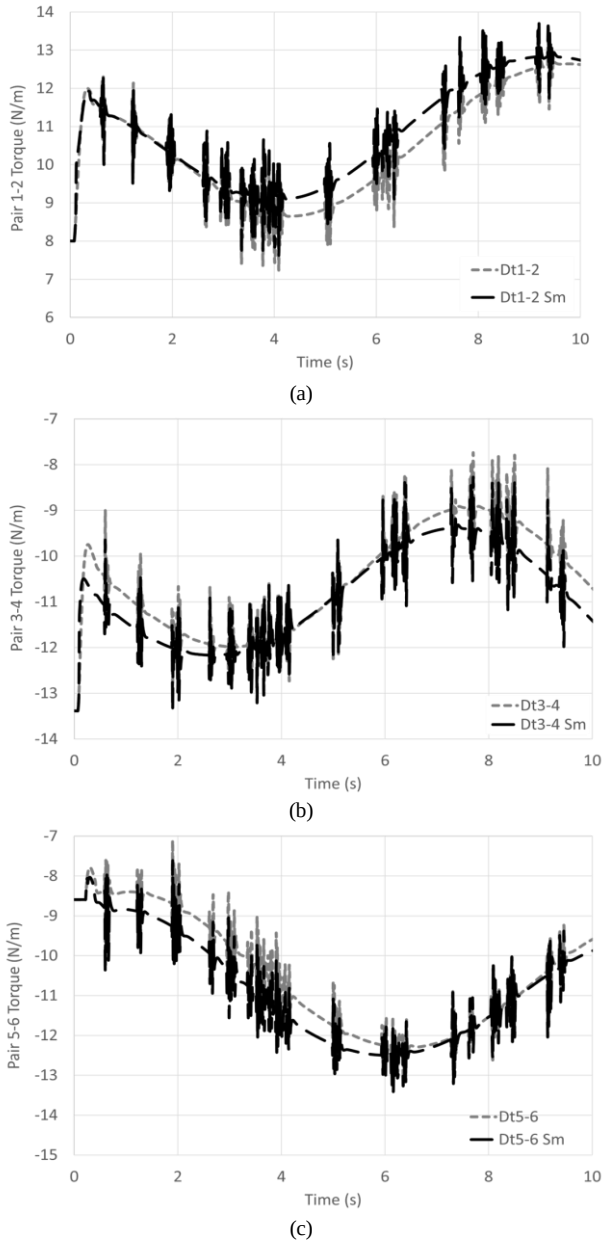

Fig. 8. Comparison between response of analytical model and simulated model of the sum of torques of the pair of actuators (a) 1 and 2. (b) 3 and 4. (c) 5 and 6.

IX. Conclusions

The similarities between the analytical model and multiphysics setting demonstrate that the plant dynamics overriding worked correctly, implying that the expressions for **M** (Eq. (96)), **C** (Eq. (97)), and **ge** (Eq. (98)) in Eq. (67) satisfactorily spanned the dynamic behavior of the mechanism. In addition, tracking the positions and rotations of the moving platform in the analytical model confirmed the model's accuracy. However, the simplifications in the pursuit of computational performance negatively affected the signal accuracy.

On the other hand, the hybrid controller, based on the response of a sliding surface considering a differential flatness strategy and an attractive signal, compensated for the structural simplification of the model. This mechanism with a symmetrical distribution allowed the actuators to work and jointly compensated for torques.

Additionally, it was shown that the dynamic model considering D'Alembert's principle and concept of virtual work is consistently applicable to control strategies for these types of parallel mechanisms. Finally, this method can be used in optimization design, which is the next step of this research.

Conflict of Interest

The authors declare no conflict of interest.

Author Contributions

Diego. Nunez: Writing and review, writing original draft, formal analysis. Mauricio. Mauledoux: Supervision, project administration, funding acquisition. Oscar. Aviles: Writing, review and methodology. Adriana. Nino: Writing, review, editing, and conceptualization. All authors had approved the final version.

Funding

This work was financially supported by the Vicerrectoría de Investigaciones, Universidad Militar Nueva Granada, under Grant IMP ING 3976 titled "Optimización de un manipulador de cinemática paralela para impresión tridimensional".

Acknowledgment

The authors wish to express their gratitude to Ariara Manrique and Sebastian Gonzalez for their technical support and advice.

References

[1] M. Dong *et al.*, "State of the Art in parallel ankle rehabilitation robot: A systematic review," *Journal of NeuroEngineering and Rehabilitation*, vol. 18, pp. 1–15, 2020. doi:10.1186/s12984-021-00845-z

[2] A. Elassal, M. Abdelaal, M. Osama, and H. Elhnidy, "Low-cost parallel delta robot for a pick-and-place application with the support of the vision system," *e-Prime-Advances in Electrical Engineering, Electronics and Energy*, vol. 8, 100518, 2024. doi: 10.1016/j.prime.2024.100518

[3] K. Xu, S. Wang, X. Wang *et al.*, "High-flexibility locomotion and whole-torso control for a wheel-legged robot on challenging terrain," in *Proc. IEEE International Conference on Robotics and Automation*, May 2020, pp. 10372–10377. doi: 10.1109/ICRA40945.2020.9197526

[4] D. A. Nunez, S. Gonzalez, J. Guacheta *et al.*, "Kinematics Parallel mechanisms design particularities focused on additive manufacturing," *Journal of Engineering Science and Technology Review*, vol. 14, no. 4, pp. 207–218, 2021. doi: 10.25103/jestr.144.25

[5] R. R. Alvarado and E. C. Castañeda, "Optimum design of the reconfiguration system for a 6-degree-of-freedom parallel manipulator via motion/force transmission analysis," *Journal of Mechanical Science and Technology*, vol. 34, no. 3, pp. 1339–1349, Mar. 2020. doi: 10.1007/S12206-020-0232-2/METRICS

[6] M. Aghaseyedabdollah, M. Abedi, and M. Pourgholi, "Interval type 2 fuzzy sliding mode control for a cable driven parallel robot with elastic cables using metaheuristic optimization methods," *Math Comput Simul*, vol. 218, pp. 435–461, Dec. 2023. doi: 10.1016/j.matcom.2023.11.036

[7] T. Sun, J. Sun, B. Lian, and Q. Li, "Sensorless admittance control of 6-dof parallel robot in human-robot collaborative assembly," *Robot Comput. Integr. Manuf.*, vol. 88, Aug. 2024. doi: 10.1016/j.rcim.2024.102742

[8] X. Jing and C. Li, "Dynamic modeling and solution of 6-DOF parallel mechanism," *IEEE Access*, vol. 10, pp. 33695–33703, 2022. doi: 10.1109/ACCESS.2022.3162367

[9] M. Pumphrey, A. Abouzarkhanifard, L. Zhang, and M. Al Janaideh, "A parallel type micro-robotic system for semi-conductor manufacturing machines: Preliminary results," in *Proc. IEEE/ASME International Conference on Advanced Intelligent Mechatronics*, AIM, pp. 532–539, Jul. 2021. doi: 10.1109/AIM46487.2021.9517669

[10] L. Milica, A. Năstase, and G. Andrei, "A novel algorithm for the absorbed power estimation of HEXA parallel mechanism using an extended inverse dynamic model," in *Proc. the Institution of Mechanical Engineers, Part K: Journal of Multi-body Dynamics*, 2020, vol. 234, no. 1, pp. 185–197. doi: 10.1177/1464419319881305

[11] B. P. Huynh and Y. L. Kuo, "Dynamic hybrid filter for vision-based pose estimation of a Hexa parallel robot," *Journal of Sensors*, vol. 2021, 9990403, Jan. 2021. doi: 10.1155/2021/9990403

[12] Z. Meng, W. Cao, H. Ding, and Z. Chen, "A new six degree-of-freedom parallel robot with three limbs for high-speed operations," *Mechanism and Machine Theory*, vol. 173, Jul. 2022. doi: 10.1016/j.mechmachtheory.2022.104875

[13] X. B. Hoang, P. C. Pham, and Y. L. Kuo, "Collision detection of a HEXA parallel robot based on dynamic model and a multi-dual depth camera system," *Sensors*, vol. 22, no. 15, 5923, Aug. 2022. doi: 10.3390/S22155923

[14] D. A. Nunez, M. Mauledoux, O. Aviles *et al.*, "Optimal design of kinematics parallel manipulator considering workspace and control," *International Journal of Mechanical Engineering and Robotics Research*, vol. 11, no. 4, 2022. doi: 10.18178/ijmerr.11.4.234-240

[15] Y. Zhao and F. Gao, "Inverse dynamics of the 6-DOF out-parallel manipulator by means of the principle of virtual work," *Robotica*, vol. 27, no. 2, pp. 259–268, Mar. 2009. doi: 10.1017/S0263574708004657

[16] A. A. Shabana, *Computational Dynamics*, 3rd ed. John Wiley & Sons, 2010.

[17] H. Sira-Ramirez and S. K. Agrawal, *Differentially Flat Systems*, 2nd ed. Boca Raton: CRC Press, 2018.

[18] V. I. Utkin, *Sliding Modes in Control and Optimization*, 2nd ed. Berlin, Heidelberg: Springer Berlin Heidelberg, 1992. doi: 10.1007/978-3-642-84379-2

[19] X. Fan, J. Ma, and R. Ji, "Integrated dynamic modeling for a stewart platform," in *Proc. Chinese Control Conference*, CCC, Oct. 2018, pp. 1844–1848. doi: 10.23919/CHICC.2018.8484101